

Experimental and Numerical Investigations on Robustness of a Deep Neural Network-based Multi-class Classification Model of CT Images with respect to Image Noise

Yuting Peng¹, Chenyang Shen², Yesenia Gonzalez², Yin Gao², Xun Jia¹

1. Department of Radiation Oncology and Molecular Radiation Sciences, Johns Hopkins University, Baltimore, MD, USA

2. Department of Radiation Oncology, University of Texas Southwestern Medical Center, Dallas, TX, USA

March 7, 2023

Abstract.

Objective: Robustness of Deep Neural Networks (DNNs) is an important aspect to consider for their clinical applications. This work examined robustness issue for a DNN-based multi-class classification model via comprehensive experimental and simulation studies.

Approach: We constructed a DNN-based multi-class classification model that classifies an axial CT image as one of the four body sites of brain & neck (BN), chest (C), abdomen & pelvis (AP), and leg & foot (LF). The model was trained with whole-body CT images of 37 patients each scanned once and 10 scans of a whole-body phantom with different mAs levels to achieve a F1 score of 99.7% averaged over four classes on a testing dataset. We evaluated robustness of the model against noise perturbations under different mAs levels using simulated CT noisy images based on noise power spectrum (NPS) and experimental CT images acquired in repeated scans of the orange-man phantom. To quantify robustness of the trained model, we defined Successful Attack Rate (SAR) as the ratio of predictions changed with noises and Confusion Matrix for Robustness (CMR) that represents the percentage of a predicted class without noise being predicted to different classes under noise. Besides, we repeatedly trained the model for 100 times using exactly the same training procedure, hyper-parameter settings, as well as the training and validation dataset to investigate robustness of models due to inherent randomness in the training process. Finally, to improve model robustness, we employed an adaptive training scheme and demonstrated its effectiveness.

Main results: Results in experimental study agreed with those of simulation study in terms of quantitatively evaluating model robustness. As mAs levels decreased, the DNN-based model showed worse robustness with respect to amplified CT noises. At 25 mAs level, SAR was 18%, 57.3%, 0%, and 28.7%,

for the BN, C, AP, and LF sites, respectively. Among 100 repeatedly trained DNN models with exactly the same setting, 14 showed robustness issue to various degrees at 25 mAs. The adaptive training scheme was effective in terms of improving model robustness, such that within two iterations model robustness issue was mitigated for both mAs levels.

Significance: Experimental and numerical studies demonstrated robustness issue of a DNN-based multi-class classification model. The discoveries highlight the needs for evaluating and ensuring DNN model robustness.

Submitted to: *Phys. Med. Biol.*

1. Introduction

Deep learning (DL) methods have attracted increasingly interests in medical domains in recent years. Employing a large-scale hierarchical multi-layer structure often in the form deep neural networks (DNNs), DL methods are extremely capable of learning feature embeddings of the data to allow state-of-the-art performance in representing the distribution followed by the data for various purposes (Kim et al., 2019; Shen et al., 2020b). With its success, DNN models have been applied to a spectrum of tasks including, but not limited to, medical image reconstruction and processing (Jiang et al., 2019; Han, 2017), disease diagnosis (Esteva et al., 2017; Lakhani and Sundaram, 2017), outcome prediction of therapeutic approaches (Ewbank et al., 2020; Men et al., 2019), radiotherapy treatment planning (Nguyen et al., 2019; Kontaxis et al., 2020; Shen et al., 2020a, 2019; Gao et al., 2022), and quality assurance (Nyflot et al., 2019; Tomori et al., 2018).

Despite these successes, understandings of DNNs' mathematical properties are few and far. Yet, it is desired to understand the DNN's properties from theoretical perspective for practical applications, as they elucidate strengths and challenges of DNN models and help ensuring validity of applications. One particular aspect of the DNN is its stability and robustness, which refers to the sensitivity of a DNN model's output with respect to small perturbations to the model's input. A DNN consists of a large number of neuron units connected under a certain structure. While the mathematical operation of each unit is simple, the end-to-end mapping established from the input to the output is extremely complex. Understanding stability of this complex mapping is critical, because in real-world applications, small perturbations to the input data are inevitable, e.g. in the form of noise, and a useful model have to be able to tolerate the noise perturbations.

Along with developments of DNN models, there have been studies demonstrating the stability and robustness concern in different applications (Drenkow et al., 2021; Laugros et al., 2019; Eykholt et al., 2018; Madry et al., 2017; Akhtar and Mian, 2018; Yuan et al., 2019). Under naturally-induced image corruptions or alternations, models sometimes may not preserve performance to confidently output correct results. Specific to the medicine domain, Finlayson et al. (2018) demonstrated the existence of perturbations to input data that can affect outputs of three representative medical DL classifiers for the classification of diabetic retinopathy from retinal funduscopy, pneumothorax from chest-xray, and melanoma from dermoscopic photographs. Shen et al. (2020c) observed the similar behavior for a DL-based classifier for lung-nodule classification from CT images (Shen et al., 2020c; Gao et al., 2021). Stability issue has also been observed for medical image

processing applications. Antun et al. (2020) investigated possible reasons for network instabilities in image reconstruction tasks. Wu et al. (2020, 2021) developed a method integrating Analytic Compressed Iterative Deep based reconstruction method and Dual-domain Residual-based Optimization Network to eliminate the instabilities. Researchers have also found that enforcing sparsity in network parameters is an effective approach to improve model robustness (Hoefer et al., 2021; Öztürk, 2021).

Previous investigations on the robustness of DNN models have been performed mostly via numerical approaches. In (Shen et al., 2020c; Gao et al., 2021), CT noise signals were sampled based on noise amplitude and a realistic noise power spectrum. Cui et al. (2021) proposed an evolution based attack method to evaluate the robustness of medical image segmentation. A recent study reported a framework for testing robustness of machine learning-based classifiers (Chuah et al., 2022). While these efforts demonstrated the model stability issue, it is desirable to have experimental studies to confirm the findings. Nonetheless, it is a practically challenging problem to assess model robustness in experimental settings. A task like this would require repeated data acquisition of the same model input under different noise realizations. Not only is this a tedious task, in some cases, this is not even feasible for ethic considerations. For instance, it is impossible to rescan a patient with CT to evaluate stability of a DNN model for CT-based disease classification. The second limitation of certain previous robustness studies is that they purposely attacked DNNs by finding specific perturbations that can alter model outputs. While these demonstrated the existence of robustness issue, the relevance to practical medical applications may be questionable, because the chance of having the specific perturbations may be small in real world. Instead, it is more meaningful to understand the robustness behavior under the naturally existing noise perturbations.

With these considered, this study evaluates the robustness of a DNN-based classification model with combined simulation and experimental approaches in an example problem that classifies an axial CT image into one of four body sites. The practical relevance of this model is that such a model often serves as the basis for subsequent tasks. For instance, for organ segmentation task, the classification model can be used to determine the body site, before calling the corresponding segmentation model Chen et al. (2021). We trained this classification model using real patient data with whole body CT scans and the data from a realistic whole body CT phantom. This setup allowed us to repeatedly scan the CT phantom to understand the stability of the classification model with respect to naturally existing CT noises.

2. Methods

2.1. DNN-based Multi-class classification model construction

We built a DNN-based multi-class classification model that classifies an axial CT image as one of four body sites: brain and neck (BN), chest (C), abdomen and pelvis (AP), leg and foot (LF). As indicated in Figure 1(a), from top to bottom, the BN site was defined as the region from the top vertex of the head to the upper lung limit. The C site included slides containing lung area. The AP site stopped at the top of femur head. The rest was defined as the LF site. We remark that the boundaries to separate adjacent regions were defined to some extent arbitrary for this study and by no means should be interpreted as accurate definitions in anatomy.

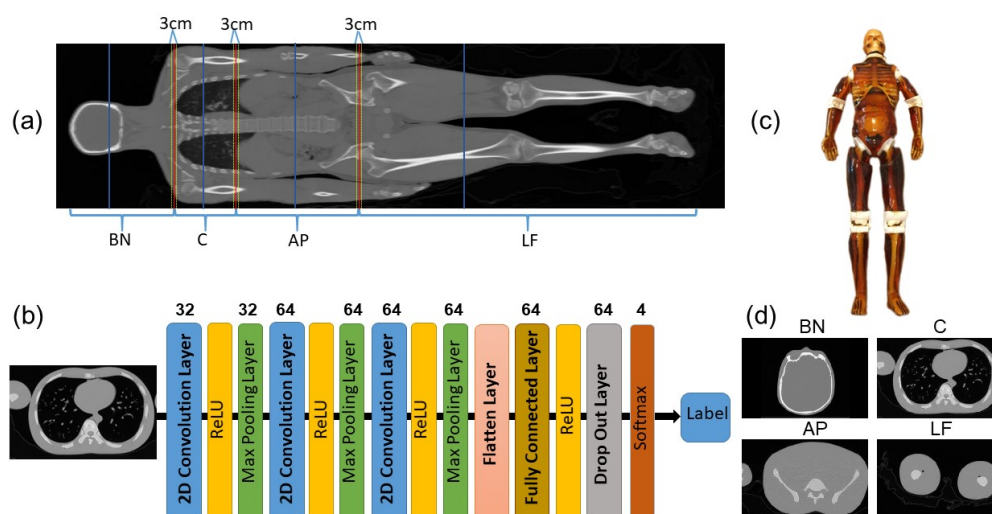


Figure 1: (a) Definition of the four body site regions, indicated by the red solid lines. Yellow dash lines are boundary regions removed when testing classification results. Blue solid lines indicate slices selected for experimental scans. (b) Structure of the DNN-based multi-class classification model. Numbers in each layer indicate the size of each layer in the constructed model. (c) Image of the orange-man phantom. (d) CT images of the phantom in experimental scans.

As shown in Figure 1(b), the DNN model followed a standard design for classification. The input was a 2D axial CT image. Three 2D convolutional layers were incorporated in the first half of the network. Each of the convolutional layers were followed by a rectified linear unit (ReLU) layer (Nair and Hinton, 2010) and a 2D max-pooling layer, to extract features from the input image. These features were

then passed through one flatten layer and two fully connected layers. One of the fully connected layers was followed by a ReLU layer. The other was utilized with a softmax activation function for the classification purpose to decide the output label $y = 1, \dots, 4$ for the four sites, respectively. Besides, we added a dropout layer before the last softmax layer to reduce overfitting (Sultan et al., 2019; Srivastava et al., 2014).

Training and testing were performed using 42790 axial CT images from whole-body CT scans of 47 patients each scanned once, and an orange-man phantom (Pure Imaging Phantoms, Farnham Royal, UK) (Figure 1(c) scanned for 20 times with different mAs levels. The whole body orange-man phantom is a human-size, full body anthropomorphic phantom with a state-of-the-art synthetic skeleton, lungs, liver, mediastinum and kidneys embedded in original soft tissue substitute. All the images were acquired on a Philips Brilliance CT scanner (Philips Healthcare, Amsterdam, Netherlands). $\sim 80\%$ (34839 samples) of CT axial images were selected for training purpose, which included CT images of 37 patients and 10 CT scans on the orange-man phantom with various mAs levels. A ten-fold cross validation (CV) strategy was implemented. The 34839 axial CT images were split into ten groups of approximately the same size by patients/phantom. For each fold, one group was picked as validation set, while the remaining samples were used for model training. Data augmentation was performed to enlarge the training dataset by randomly scaling the CT images with factors in $80 \sim 120\%$.

The DNN models were trained by solving the following optimization problem:

$$\theta^* = \arg \min_{\theta} \sum_{i \in T} \|D(x_i|\theta) - y_i^*\|_2^2, \quad (1)$$

where x_i represents the i -th CT image in the training dataset. y_i^* is the ground truth label for x_i . $D(x_i|\theta)$ represents the DNN function with θ being the network parameter set to be determined. The optimization problem was solved using the adaptive moment estimation (Adam) algorithm (Kingma and Ba, 2014) with Python with TensorFlow. The models were trained with 20 epochs using a batch size of 64 and an learning rate of 1×10^{-4} . These hyper-parameters were manually adjusted for the best performance. All the computations were implemented on a radiation oncology high performance computing server at UT Southwestern medical center.

After training, the model was tested using the remaining 20% data ($N_{test} = 7951$) that were unseen by the training process. The performance was evaluated using metrics including precision, recall and F1-score for the specified classes. One issue in the evaluation was the to some extent ambiguously defined boundaries between body sites. To mitigate this impact, we also performed a test using a dataset by removing a transition zone at each boundary, as indicated by the yellow dashed lines in Figure

1 (a)). The transition zone was defined as a region of six CT slices (3 cm) centering at each boundary slice. Among the models trained from the 10-fold CV study, the one with the highest F1-score averaging over the four classes in the independent test was advanced to the next step for robustness evaluations.

2.2. DNN-based Multi-class classification model robustness evaluation

Once the DNN model’s performance was confirmed, we evaluated its robustness with respect to realistic CT noises in the input. We focused the study on the orange-man phantom, which allowed us to perform both numerical simulation and experimental studies. For the trained model, let Y_i denote the model’s predicted label for an unperturbed input axial CT image X_i . For each X_i , we could add realistic (via simulations or experiments) CT noises and fed the perturbed images into the DNN to output the new predicted label, denoted as Y_i' . Evaluation of Y_i' for X_i with noise added is called attack. An attack is considered successful, if $Y_i \neq Y_i'$. A reliable multi-class classification model is expected to be robust against noise perturbations.

To quantify the model’s robustness, a metric Successful Attack Rate (SAR) was introduced. For a given body site i , SAR was determined as:

$$SAR_i = \frac{N_{succ}^i}{N_{attack}^i}(\%), \quad (2)$$

where N_{succ}^i represents the number of successful attacks and N_{attack}^i is the total number of attacks. The lower SAR is, the more robust the DNN model is.

We also computed Confusion Matrix for Robustness (CMR) for the multi-classification model. Different from the confusion matrix commonly used to represent the percentage of an actual class being predicted to different classes, CMR represents the percentage of a predicted class without noise being predicted to different classes under noise. The matrix is of a size 4×4 in this study corresponding to the four body sites. An identity matrix indicates the most robust case with the predictions unaffected by noise. Note that for each column i corresponding to a given body site, sum of off-diagonal elements equals to SAR_i by definition.

2.2.1. Generating samples in simulation study

For numerical simulation, while our previous study used simulated CT noise to evaluate model robustness (Shen et al., 2020c), the noise was generated for a single patch from a given noise power spectrum (NPS). Yet it is known that CT noise is non-stationary and spatially correlated, the current study utilized an image domain noise insertion method to generate a whole image noise to investigate DNN robustness in a more realistic setting (Divel and Pelc, 2019). In particular, we aimed at generating

realistic CT noise for the orange-man phantom, so that we could compare numerical study results with those of experimental studies.

As such, we selected one slice of interest from each body region in the orange-man phantom denoted by the blue solid line in Figure 1(a). The slice of interest in each body site located in the middle region of each body site. This choice was made to allow us focusing on the evaluations of DNN model’s robustness, as robustness of slices close to the boundary between two adjacent sites may be affected by ambiguity of defining a body site. For a CT slice of interest, we first repeatedly scan the phantom for 20 times at a reference mAs level of 25 mAs to estimate its NPS. The repeated CT images shared the same structure but different noise realizations. We obtained the average CT image and the noise realizations by subtracting the average image from each CT image. After that, we divided the image region into overlapping patches, within which the noise was assumed to be stationary. The size of patches was $6.8 \text{ mm} \times 6.8 \text{ mm}$, and they were overlapped by 30% to avoid discontinuities at the boundaries. The NPS in a patch was estimated using the ensemble average of the power spectrum from multiple acquisitions (Siewerdsen et al., 2002), as

$$S(f_x, f_y|x, y) = \frac{\Delta_x \Delta_y}{N_x N_y} \langle |\mathcal{F}(n(x, y))|^2 \rangle, \quad (3)$$

where f_x, f_y are the frequencies in the Fourier space, Δ_x and Δ_y are pixel sizes, and N_x and N_y are the number of pixels. $n(x, y)$ is the noise signal of each acquisition, \mathcal{F} denotes the Fourier transform, and $\langle \cdot \rangle$ indicates the ensemble average.

With the NPS calculated for each patch, we generated the spatially correlated CT noise across the whole CT image. Specifically, a white normal Gaussian noise was constructed for an image that has the same matrix size as the CT image. Then the white noise was filtered in the image domain by $s(x, y) = \mathcal{F}^{-1} \sqrt{S(f_x, f_y)}$, the inverse Fourier transform of the square root of the estimated NPS $S(f_x, f_y|x, y)$ in Eq. (3), to achieve the proper spatial correlation within each patch. Note that these small patches were overlapped with each other. To obtain the complete image of a CT noise, we merged noise data in overlapped regions between adjacent patches using a weighted scheme with a trapezoidal windowing function. Finally, we scaled the noise amplitude corresponding to a targeted mAs level with a factor α as following:

$$\alpha = \frac{\sigma(mAs)}{\sigma(mAs_0)} = \sqrt{\frac{mAs_0}{mAs}}, \quad (4)$$

to account for the difference in CT noise standard deviation σ between the reference mAs level (mAs_0 , 25 mAs in this study) and the targeted mAs level.

Using this method, we generated 1000 noise images under each specific mAs level in a wide mAs ranging from 12.5 mAs to 500 mAs for each slice of interest. Adding the noises to the average CT image yielded simulated CT images with realistic noises.

2.2.2. Generating samples in experimental study

As it is not possible to repeatedly scan patients, we used the orange-man phantom as an alternative to evaluate the robustness of DNN-based models. As such, we repeatedly scanned the phantom at the four slices of interest. The mAs level affects noise amplitude and hence has a significant influence on the model prediction robustness. Generally speaking, increasing mAs increases radiation dose of the CT scan and decreases the amount of noise, hence improving the contrast resolution of the image. Balancing the dose with the contrast resolution required for interpretation must be considered when determining examination settings. In this study, we performed experimental scans under 200 mAs and 25 mAs levels. The 200 mAs level is a commonly used level in our clinic for high quality scans. The lowest mAs level available at our scanner is 25 mAs, which was hence chosen to study model robustness in a high-noise setting. The lowest mAs setting with the largest noise magnitude also represents a typical setup for the low dose CT scan, e.g. for screening purpose. For a particular mAs level, e.g. 25 mAs, the experimental CT scans were performed 150 times repeatedly on each of the four body sites, respectively. During the repeated scans, all the CT acquisition parameters and settings such as field of view, and slice thickness were kept the same.

2.3. Robustness evaluations

With the simulation and experimental data acquired, we fed the data to the DNN model. SAR and CMR were computed to evaluate model robustness.

It is also necessary to compare the results from experimental scans and simulated CT noise images. This was achieved via a statistical test. Specially, each entry of the CMR represents the probability $p_{i,j}$ of a given class j predicted for noiseless CT images being predicted to a class i under noise perturbations, for $i, j = 1, \dots, 4$. They was estimated based on repeated experiments via numerical simulations as $\hat{p}_{i,j}^1$ or actual CT scans as $\hat{p}_{i,j}^2$, but the corresponding true values $p_{i,j}^1$ and $p_{i,j}^2$ were unknown. We performed the test with the null hypothesis that $p_{i,j}^1 = p_{i,j}^2$. Assuming the DNN prediction results under noise perturbations follow a binomial distribution, and under normal approximation to binomial distribution given the relatively large sample sizes, we computed Z value as $Z_{i,j} = \frac{p_{i,j}^1 - p_{i,j}^2}{\sqrt{p_{i,j}(1-p_{i,j})(\frac{1}{n_1} + \frac{1}{n_2})}}$, where $p_{i,j} = \frac{n_1 p_{i,j}^1 + n_2 p_{i,j}^2}{n_1 + n_2}$, and $n_1 = 1000$ and $n_2 = 150$ are the number of experiments in simulation and phantom studies, respectively. We may reject the null hypothesis, if $|Z_{i,j}|$ is larger than the critical region value $Z^* = 1.96$ with 95% confidence level in this two tailed test problem.

In addition, we also studied the robustness issue in two other aspects.

2.3.1. Robustness of models trained under the same training scheme

The training process for a DNN model often inherently contains randomness. Even with the same training data and same hyper-parameter setting, the randomness occurs due to stochastic operations during the training process, such as the stochastic gradient descent method that randomly select a subset of training data at each optimization step. As such, the resulting models are not the same, and it is hence important to understand the robustness distribution of these models. For this purpose, we performed an evaluation study on the robustness of multiple models trained under the same setting. We repeatedly trained the multi-class classification model for 100 times using exactly the same training procedure, settings, as well as the training and validation dataset. We then evaluated the robustness of these 100 models using experimentally acquired CT images.

2.3.2. Adaptive training approach to improve robustness

In a previous study, we proposed an adaptive training scheme that improved the DNN-based models' robustness (Shen et al., 2020c) by repeatedly fine-tuning the DNN-based model. At each iteration, the scheme evaluated robustness of the trained DNN using simulated data with realistic noise perturbations, and then retrained the DNN model by adding to the training dataset those perturbations that successfully altered the DNN's output. While our previous study demonstrated the effectiveness of this approach, only simulation studies were conducted. Here, we studied the effectiveness of the adaptive training scheme using experimental data. Specifically, we followed the proposed adaptive training scheme using simulation data to generate perturbations and retrain the model. In parallel to this process, we used the experimental data to measure robustness of the model and monitor the improvement. This is expected to serve as a ground truth way to show the validity of the adaptive training scheme.

3. Results

3.1. DNN model's performance

While model performance was not the focus of this study, we presented it here to ensure that subsequent robust analysis was built on models with reasonable performance. The precision, recall and F1-score for the DNN-based multi-class classification models obtained in the 10-fold CV scheme are listed in Table 1. The

results are the average and standard deviations over the ten models, showing their excellent performance. Testing 1 and 2 are independent tests using the whole testing data, and using the data without the transition zone between neighboring body sites, respectively. Note that the performance in Testing 2 was better than that of Testing 1, because of the removal of ambiguity of anatomy at the transition zones. Among the 10 models in the CV scheme, the model with the highest F1-score averaging over the four classes for the Testing 2 dataset was used to evaluate the robustness in the remaining of this paper.

Table 1: Multi-class classification performance on training, validation and testing datasets. Each result is average and standard deviations estimated over the ten-fold CV study. All numbers are in %.

Datasets	Metrics	BN	C	AP	LF
Training	Precision	99.8±0.3	99.5±0.4	99.8±0.2	99.9±0.0
	Recall	99.8±0.2	99.6±0.4	99.9±0.1	100±0.0
	F1-score	99.8±0.1	99.5±0.2	99.9±0.0	100±0.0
Validation	Precision	97.9±1.9	95.9±2.4	98.1±1.2	99.4±0.7
	Recall	98.5±1.3	96.8±1.7	98.1±1.5	99.2±0.9
	F1-score	98.2±1.1	96.3±1.2	98.1±0.9	99.3±0.4
Testing 1	Precision	99.3±0.7	96.0±1.2	98.1±0.6	99.7±0.2
	Recall	98.5±0.6	95.8±1.7	98.8±0.4	99.5±0.2
	F1-score	98.9±0.2	95.9±0.5	98.5±0.2	99.6±0.1
Testing 2	Precision	99.7±0.5	99.7±0.3	99.5±0.4	100±0.0
	Recall	100±0.0	98.0±1.1	100±0.0	100±0.0
	F1-score	99.8±0.3	98.8±0.5	99.7±0.2	100±0.0

3.2. Noise generation

We first demonstrated validity of the simulation approach to generate realistic noises by comparing the noise images and noise standard deviation images obtained in actual CT scans and simulations. As shown in Figure 2 (a-f), the simulated noise possessed visually a similar pattern as the noise in the experimental CT scan. The standard deviation images were calculated over 20 experimental CT noises and 20 simulated realistic noises. They both exhibited close correlations with the underlying anatomical features, as well as similar variance maps. It is difficult to quantitatively measure the statistical agreement between the simulated and actual noise signals.

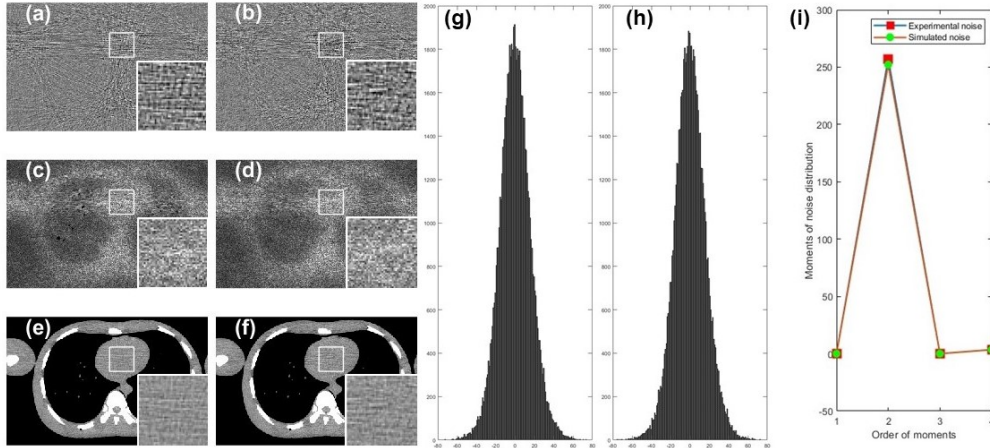


Figure 2: (a)-(b) CT noise images for CT scans and simulated noise under 25 mAs. Display window is $[-80, 80]$ HU. (c)-(d) CT noise standard deviations for CT scans and simulated noise under 25 mAs. Display window is $[0 40]$ HU. The white boxes are zoomed-in regions. (e)-(f) Experiment CT image and image with simulated noise under 25 mAs. Display window is $[-200 200]$ HU. (g)-(h) Histograms of noise images for CT scans and simulated CT images. (i) Comparisons of moments of noise distributions for CT scans and simulated CT images.

As a means for demonstration, we plot histograms of the noises in Figure 2 (g) and (h). We also computed up to the 4th order of moment of the two distributions as in Figure 2 (i). The differences were within 2%, reflecting agreement between the two.

3.3. Robustness evaluations

3.3.1. Robustness of trained model In the simulation study, we generated 1000 simulated noise images at each of the four body sites for the orange-man phantom under different mAs levels ranging from 12.5 mAs to 500 mAs. SAR of the DNN-based model for the four body sites were calculated and the results are summarized in Figure 3(a). First, generally speaking, the robustness of DNN output results became worse with reduced mAs level. This is expected, as lowering the mAs level resulted in increased noise levels and hence large perturbations to the input CT images that tend to increase the chance of changing the DNN's outputs. Second, different classes attained robustness to different degrees. The class AP was found to be the most robust with respect to noise perturbations. All the predicted results kept unchanged with noise perturbations, and SAR for this class was zero. However, the other three classes (BN, C and LF) showed significantly weaker robustness. In Figure 3 (b) and (c), the plots of SAR were displayed in zoomed-in views under the mAs ranges

from 50 mAs to 12.5 mAs, and 225 mAs to 175 mAs, respectively. It was observed that under 200 mAs, the LF class was robust against the noise perturbations, with SAR being zeros. As mAs was reduced, it became sensitive to noise perturbations starting from 100 mAs level, where SAR started to be non-zero. For BN and C classes, robustness issue started to appear from 225 mAs and 325 mAs, respectively. At the large noise limit of 12.5 mAs, SAR of BN, C, and LF were 88.6%, 72.5%, and 41.2%, respectively.

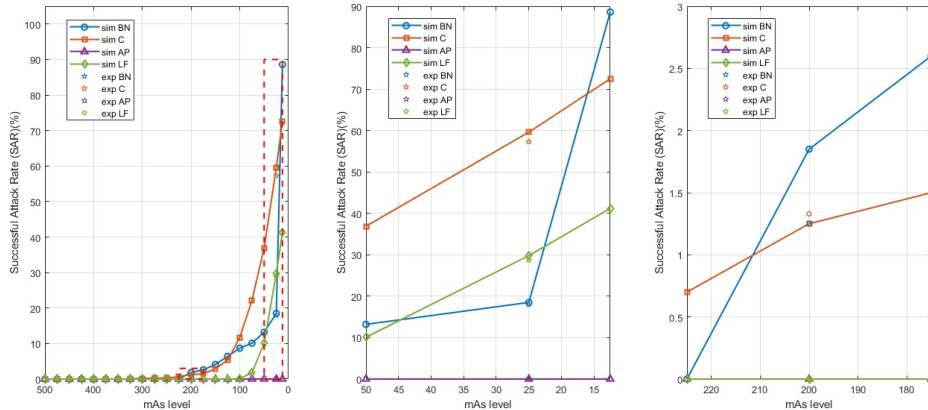


Figure 3: (a) SAR with respect to CT noises under different mAs levels (from 12.5 mAs to 500 mAs). Marker stars denoted the SAR for experimental studies under 200 mAs and 25 mAs, respectively. Rectangular boxes indicated the zoomed-in regions in (b-c). (b) Zoom-in view of plots for mAs range in [12.5, 50] mAs. (c) Zoom-in view of plots for mAs range in [175, 225] mAs.

As for the experimental studies, the results shown as star markers in Figure 3 generally agreed with the simulation results. At 200 mAs level, SAR for the BN and C sites both were 1.25%, while for the AP and LF sites, SAR were zeros. However, under 25 mAs level, SAR for the BN, LF, and C sites increased to 18%, 28.7%, and 57.3%, while that for the AP site remained at zero. These experimentally obtained SARs were consistent with those computed by the simulated CT noise perturbations, as shown in Figure 3.

In Figure 4, the CMRs are presented for experimental and simulation studies at 200 mAs and 25 mAs. At 200 mAs, the C and BN sites appeared to be slightly not robust. For instance, in the experimental study, majority of the C site was still predicted as the C site with noise perturbations, but with 1.33% probability the prediction was incorrectly as AP. This number was close to the simulation result in Figure 3, where SAR of simulated CT chest axial images at 200 mAs was 1.25%;

while under 25 mAs, 86 of 150 CT chest scans were predicted as AP site, resulting in the experimental SAR value of 57.33%, which was close to the simulated SAR value of 59.6%.

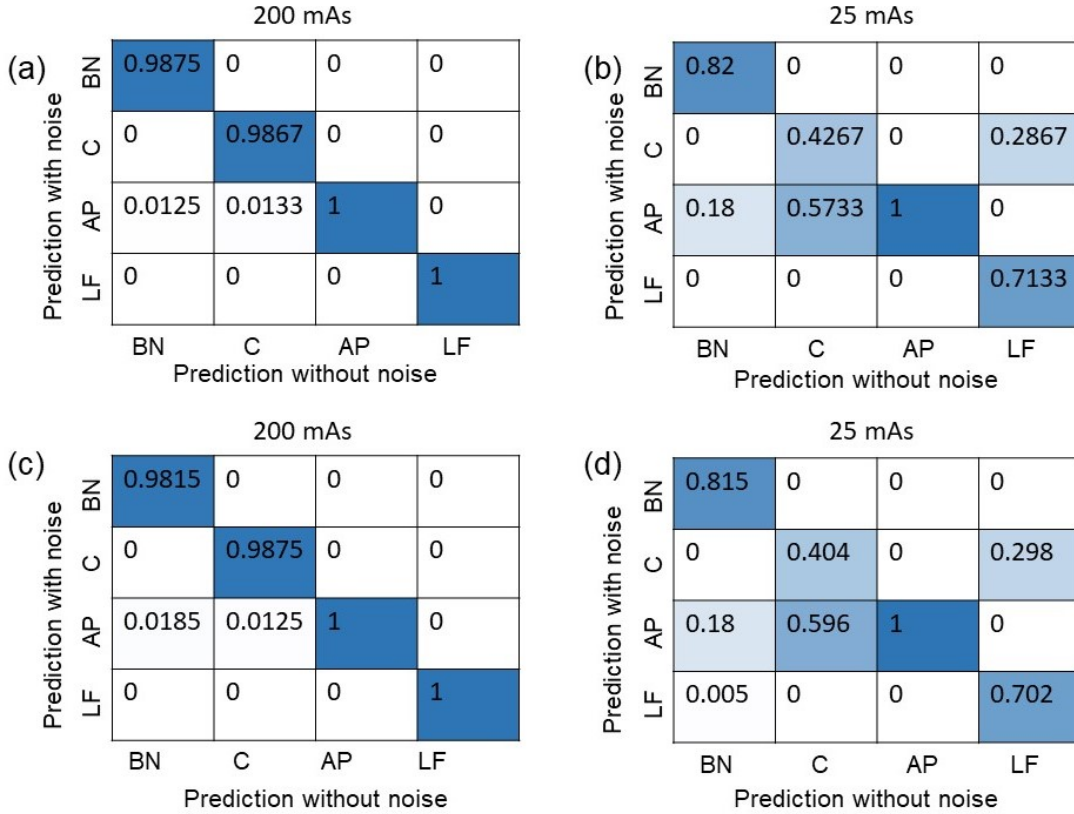


Figure 4: CMR of (a) experimental study at 200 mAs; (b) experimental study at 25 mAs; (c) simulated study at 200 mAs; and (d) simulated study at 25 mAs.

To compare the experimental and simulation results, Figure 5 presents Z values for 200 mAs and 25 mAs. All the $|Z|$ values were less than the critical value $Z^* = 1.96$. Hence, at the 95% confidence level, we cannot reject the null hypothesis testing that the corresponding entries in CMRs calculated by experimental studies and by numerical simulations are statistically the same.

3.4. Robustness of models trained under the same training scheme

As described in Section 2.3.1, we repeatedly trained the DNN-based classification models for 100 times using the same setup. The precision, recall and F1-score of each DNN model obtained for the testing dataset without axial CT images at boundaries

		200 mAs						25 mAs					
(a)	Prediction with noise	BN	0.5194	0	0	0	(b)	Prediction with noise	BN	0.1473	0	0	0
		C	0	-0.0819	0	0			C	0	0.5227	0	-0.2826
		AP	-0.5194	0.0819	0	0			AP	0	-0.5227	0	0
		LF	0	0	0	0			LF	-0.8679	0	0	0.2826
		BN	C	AP	LF			BN	C	AP	LF		
		Prediction without noise						Prediction without noise					

Figure 5: Test statistics of the null hypothesis testing that the calculated CMRs of experimental scans and simulated CT noisy images were statistically same with each other under (a) 200 mAs and (b) 25 mAs.

between adjacent body site regions (Testing2 in Table 1) were calculated. The mean value of precision over the 100 trained DNN models for BN, C, AP and LF classes were 99.6%, 99.4%, 99.1% and 98.8%, the averaged recall were 100%, 98.6%, 99.9% and 99.5%, and the averaged F1-score were 99.9%, 98.8%, 99.6% and 99.2%, respectively. These high values showed excellent performance of the 100 DNN-based models on multi-class classification for the testing dataset.

Subsequently, we performed the robustness study on the 100 well-trained DNN models using the experimental scans. The results are shown in Figure 6. Out of the 100 DNN models, 14 models exhibited robustness issue with non-zero SAR for BN, C and LF sites under 25 mAs. We summarized the CMRs of all the 100 models by presenting the element-wise mean values and standard deviations. As seen in Figure 6 (a) and (c), both of the averaged CMRs under 200 mAs and 25 mAs showed non-zero off-diagonal elements, with the amplitudes of off-diagonal elements increased with noise. SAR for the BN, C, AP and LF sites at 200 mAs were 2.37%, 0%, 0, and 1.59%, respectively; and those at 25 mAs were 5.21%, 1.23%, 0%, and 3.36%, respectively. Figure 6 (b) and (d) showed the standard deviations of 100 CMRs. Under 25 mAs, the standard deviations of CMRs were larger than those under 200 mAs. These results demonstrated that even though the 100 DNN-based models were trained in exactly the same training scheme and dataset, because of the inherent randomness during the training process, the results had different level of robustness. Similar to the previous findings, these 100 models on exhibited different robustness extent on the four classes. Among the four body sites, prediction on the AP site was found to be much more robust than the other three sites.

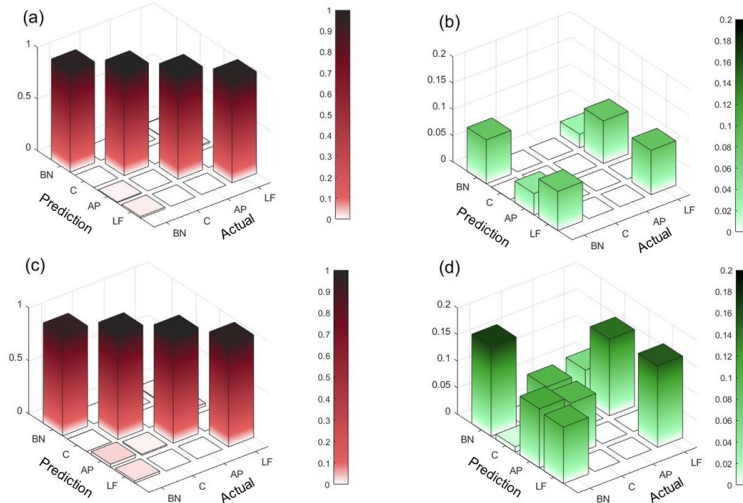


Figure 6: 3D view for (a) mean and (b) standard deviation of CMRs of 100 DNN-based models against CT scans under 200 mAs; (c) mean and (d) standard deviation of CMRs of 100 DNN-based models against CT scans under 25 mAs.

3.5. Adaptive training scheme to improve robustness

We employed the adaptive training scheme to improve the DNN models' robustness in this study. Experimental study results on the robustness of the adaptively trained DNN models are presented in Figure 7. As the perturbed samples that successfully attacked the trained network were added to the training dataset, the newly trained DNN model showed significantly improved robustness. Specifically, for the 200 mAs case, SAR for BN and C sites were reduced to zeros after the adaptive training scheme was applied with one iteration. For the 25 mAs case, SAR for BN and LF sites were reduced to zeros at the first iteration, while SAR for C site was reduced to 15.3% from 57.3%. After two iterations, SARs for all sites became zero. In Figure 7 (f), the averaged SARs over all sites are plotted against the number of iterations for the two mAs levels. The monotonically decaying trend of the two curves indicated validity of the adaptive training scheme to improve model robustness.

Additionally, we further tested the adaptively trained DNN models after two iterations using the numerically simulated CT images at four body sites under mAs levels from 500 mAs to 12.5 mAs. It was found that SARs for all the considered cases were reduced to zeros.

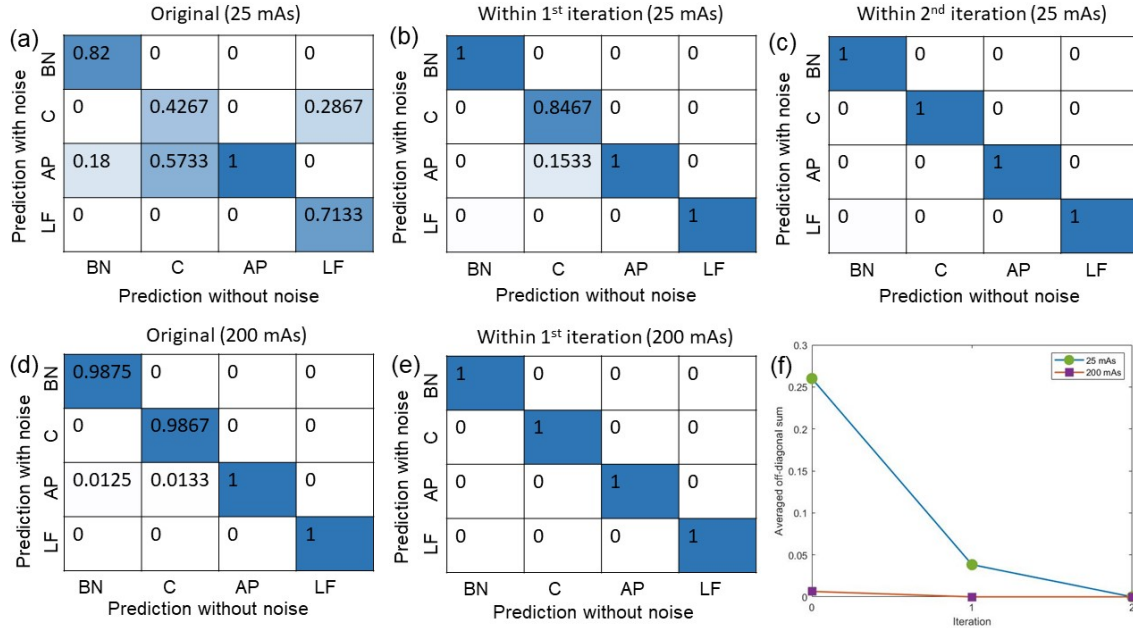


Figure 7: (a)-(c) CMRs during the adaptive training process for 25 mAs level. (d)-(e) CMRs during the adaptive training process for 200 mAs level. (f) Averaged off-diagonal sums over all sites during the adaptive training process.

4. Discussions

Robustness is a critically important aspect to consider, when developing DNN models for clinical applications. Our group, and others, have previously investigated robustness of DNN models in extensive studies (Shen et al., 2020c; Gao et al., 2021; Cui et al., 2021; Antun et al., 2020; Wu et al., 2020, 2021). Compared to existing studies, the current work is different in the following aspects, which hence highlights the contributions of this study.

First, this study employed the simulation approach to study the robustness of DNN-based multi-class classification models by generating the simulated realistic CT noises in the entire image domain. While our previous study (Shen et al., 2020c) generated CT noises via simulation for robustness evaluation, noise was conducted at a patch level, and hence the simulated CT noise ignored position dependent of NPS, a well-known property of the CT image noises. The current study overcame this limitation by generating noise images considering NPS variations through the image domain. Our experimental studies validated the accuracy of generated noise signal.

Second, to our knowledge, this is the first time that a comprehensive study including both simulation and experimental investigations were performed to demonstrate the robustness issue of a DNN-based classification model in a clinically relevant problem. We conducted the study with repeatedly scans of the orange-man phantom at a few slices under various mAs levels. The robustness measure in terms of SAR and CMR were found to be quantitatively in agreement between the simulation and the experimental studies. The experimental study served as a ground truth approach to demonstrate robustness issue of a well-trained DNN classification model, as well as to show the validity of simulations to investigate the robustness issue.

Third, this study focused on naturally existing noise in CT images. Robustness concern DNN-based classification model has been long studied in general. Yet, although it has been demonstrated in different contexts, most existing studies focused on attacking DNN models, namely to purposely identify perturbations that can manipulate DNN model outputs (Eykholt et al., 2018; Laugros et al., 2019; Akhtar and Mian, 2018; Yuan et al., 2019; Finlayson et al., 2018). While those studies undoubtedly showed existence of perturbations capable of affecting DNN model performance, the clinical relevance may be questioned, as the purposely constructed perturbations may not exist at a high chance. Different from these studies, the perturbations in this work were sampled from the actual CT image noise domain, via simulations or experiments. The robustness concern of the trained DNN model under these noise perturbations made our study more relevant to real clinical applications.

Last, in addition to evaluating robustness for one trained model, we also investigated variations of robustness among models trained under the same setting. The variation of robustness is a valid concern. Due to randomness in model training caused by the stochastic nature of the numerical algorithm, while the resulting trained model all achieved a satisfactory level of classification performance, we found that they may behave with different levels of robustness. Ultimately, a DNN model represents a highly non-linear function mapping between an input CT image and a classification label, whose output may be sensitive to input image values. Due to the highly non-convex optimization problem of DNN model training, the resulting DNN models under repeated training runs are local minima of the objective function, which attain different numerical properties. Our study revealed the variation of robustness among them, hence highlighting the need for assessing model robustness on a case-by-case bases.

Meanwhile, our study has the following limitations. As DNNs have been widely used in a broad scope with different network setups for applications etc, we would like to remark on the validity of the study to avoid over-interpreting the results.

First of all, while using the phantom allowed us to demonstrate the robustness issue via a real experimental setting, strictly speaking, our study only showed the existence of the robustness concern, when classifying a CT slice of the phantom. The existence of this problem in real patient case was still unverified. Yet we hope the realistic appearance of the orange-man phantom relative to real humans in CT image can support the use of the phantom as a surrogate to investigate the robustness problem for real patient cases. Moreover, as our study, e.g. the statistical test, showed validity of using simulations as a means for robustness study, we will perform more studies with simulated noise perturbations to comprehensively investigate the problem in patient cases.

Another limitation is the relevance of the selected classification problem, i.e. body site identification, to the actual clinical problems of interest, for instance lung nodule classification. As mentioned previously, we chose the body site identification problem for the purpose to allow experimental studies on a physical phantom. Yet, for this classification task, it is expected that the trained DNN model may extract image features at the body scale, such as cross section size and shape, to decide the classification label. The feature selection may not be of relevance to lung nodule classification problem, which focuses on small scale features for the nodules. Hence, the robustness concern identified from this study may not be generalizable to the lung nodule classification problem. We expect that phantom studies with realistically 3D printed nodules may be performed to evaluate robustness issue for the lung nodule classification problem (Hatamikia et al., 2023), although it may be a challenge to replicate nodules of different categories.

Third, this work only studied the robustness on one network model with a very specific and relatively simple network structure for multi-class classification purpose. It is expected that the robustness level depends on many factors such as specific model structure and model training process. Hence, it should be understood that the observed behaviors are for the model studied here, whereas generalization of the discoveries to other models may not hold. With the rapid progress of DL, advanced models have been explored, such as transformer (Willemink et al., 2022), diffusion model (Kazerouni et al., 2022) etc. There have been initial studies on the robustness of these models. It is our ongoing work to evaluate these models' robustness using the simulation and experimental approaches developed in the current study.

5. Conclusion

In this paper, we investigated robustness of a multi-class classification DNN-based model with respect to CT noises via simulation and experimental approaches. The

results in experimental study agreed with those in simulations, both showed that the DNN model had robustness issue to CT noises to the degree depending on mAs levels. We also demonstrated that repeatedly trained DNN models with exactly the same training scheme attained different levels of robustness, and that the adaptive training scheme is effective in terms improving robustness of the DNN model.

Acknowledgement

This work was funded in part by the National Institutes of Health under the grants R37CA214639, R01CA227289, R01CA237269, R01EB032716, and R01CA254377.

References

- Naveed Akhtar and Ajmal Mian. Threat of adversarial attacks on deep learning in computer vision: A survey. *IEEE Access*, 6:14410–14430, 2018.
- Vegard Antun, Francesco Renna, Clarice Poon, Ben Adcock, and Anders C Hansen. On instabilities of deep learning in image reconstruction and the potential costs of ai. *Proceedings of the National Academy of Sciences*, 117(48):30088–30095, 2020.
- Xuming Chen, Shanlin Sun, Narisu Bai, Kun Han, Qianqian Liu, Shengyu Yao, Hao Tang, Chupeng Zhang, Zhipeng Lu, Qian Huang, et al. A deep learning-based auto-segmentation system for organs-at-risk on whole-body computed tomography images for radiation therapy. *Radiotherapy and Oncology*, 160:175–184, 2021.
- Joshua Chuah, Uwe Kruger, Ge Wang, Pingkun Yan, and Juergen Hahn. Framework for testing robustness of machine learning-based classifiers. *Journal of Personalized Medicine*, 12(8), 2022. ISSN 2075-4426. doi: 10.3390/jpm12081314. URL <https://www.mdpi.com/2075-4426/12/8/1314>.
- Xiangxiang Cui, Shi Chang, Chen Li, Bin Kong, Lihua Tian, Hongqiang Wang, Peng Huang, Meng Yang, Yenan Wu, and Zhongyu Li. Deattack: A differential evolution based attack method for the robustness evaluation of medical image segmentation. *Neurocomputing*, 465:38–52, 2021.
- Sarah E Divel and Norbert J Pelc. Accurate image domain noise insertion in ct images. *IEEE Transactions on Medical Imaging*, 39(6):1906–1916, 2019.
- Nathan Drenkow, Numair Sani, Ilya Shpitser, and Mathias Unberath. Robustness in deep learning for computer vision: Mind the gap? *CoRR*, abs/2112.00639, 2021. URL <https://arxiv.org/abs/2112.00639>.
- Andre Esteva, Brett Kuprel, Roberto A Novoa, Justin Ko, Susan M Swetter, Helen M Blau, and Sebastian Thrun. Dermatologist-level classification of skin cancer with deep neural networks. *nature*, 542(7639):115–118, 2017.

- Michael P Ewbank, Ronan Cummins, Valentin Tablan, Sarah Bateup, Ana Catarino, Alan J Martin, and Andrew D Blackwell. Quantifying the association between psychotherapy content and clinical outcomes using deep learning. *JAMA psychiatry*, 77(1):35–43, 2020.
- Kevin Eykholt, Ivan Evtimov, Earlene Fernandes, Bo Li, Amir Rahmati, Chaowei Xiao, Atul Prakash, Tadayoshi Kohno, and Dawn Song. Robust physical-world attacks on deep learning visual classification. In *Proceedings of the IEEE Conference on Computer Vision and Pattern Recognition*, pages 1625–1634, 2018.
- Samuel G Finlayson, Hyung Won Chung, Isaac S Kohane, and Andrew L Beam. Adversarial attacks against medical deep learning systems. *arXiv preprint arXiv:1804.05296*, 2018.
- Yin Gao, Jennifer Xiong, Chenyang Shen, and Xun Jia. Improving robustness of a deep learning-based lung-nodule classification model of ct images with respect to image noise. *Physics in Medicine & Biology*, 66(24):245005, 2021.
- Yin Gao, Chenyang Shen, Yesenia Gonzalez, and Xun Jia. Modeling physician’s preference in treatment plan approval of stereotactic body radiation therapy of prostate cancer. *Physics in Medicine & Biology*, 67(11):115012, 2022.
- Xiao Han. Mr-based synthetic ct generation using a deep convolutional neural network method. *Medical physics*, 44(4):1408–1419, 2017.
- Sepideh Hatamikia, Ingo Gulyas, Wolfgang Birkfellner, Gernot Kronreif, Alexander Unger, Gunpreet Oberoi, Andrea Lorenz, Ewald Unger, Joachim Kettenbach, Michael Figl, et al. Realistic 3d printed ct imaging tumor phantoms for validation of image processing algorithms. *Physica Medica*, 105:102512, 2023.
- Torsten Hoeffler, Dan Alistarh, Tal Ben-Nun, Nikoli Dryden, and Alexandra Peste. Sparsity in deep learning: Pruning and growth for efficient inference and training in neural networks. *arXiv preprint arXiv:2102.00554*, 2021.
- Zhuoran Jiang, Yingxuan Chen, Yawei Zhang, Yun Ge, Fang-Fang Yin, and Lei Ren. Augmentation of cbct reconstructed from under-sampled projections using deep learning. *IEEE transactions on medical imaging*, 38(11):2705–2715, 2019.
- Amirhossein Kazerooni, Ehsan Khodapanah Aghdam, Moein Heidari, Reza Azad, Mohsen Fayyaz, Ilker Hacihaliloglu, and Dorit Merhof. Diffusion models for medical image analysis: A comprehensive survey. *arXiv preprint arXiv:2211.07804*, 2022.
- Mingyu Kim, Jihye Yun, Yongwon Cho, Keewon Shin, Ryoungwoo Jang, Hyun-jin Bae, and Namkug Kim. Deep learning in medical imaging. *Neurospine*, 16(4):657, 2019.

- Diederik P Kingma and Jimmy Ba. Adam: A method for stochastic optimization. *arXiv preprint arXiv:1412.6980*, 2014.
- C Kontaxis, GH Bol, JJW Lagendijk, and BW Raaymakers. Deepdose: Towards a fast dose calculation engine for radiation therapy using deep learning. *Physics in Medicine & Biology*, 65(7):075013, 2020.
- Paras Lakhani and Baskaran Sundaram. Deep learning at chest radiography: automated classification of pulmonary tuberculosis by using convolutional neural networks. *Radiology*, 284(2):574–582, 2017.
- Alfred Laugros, Alice Caplier, and Matthieu Ospici. Are adversarial robustness and common perturbation robustness independent attributes? In *Proceedings of the IEEE/CVF International Conference on Computer Vision Workshops*, pages 0–0, 2019.
- Aleksander Madry, Aleksandar Makelov, Ludwig Schmidt, Dimitris Tsipras, and Adrian Vladu. Towards deep learning models resistant to adversarial attacks. *arXiv preprint arXiv:1706.06083*, 2017.
- Kuo Men, Huaizhi Geng, Haoyu Zhong, Yong Fan, Alexander Lin, and Ying Xiao. A deep learning model for predicting xerostomia due to radiation therapy for head and neck squamous cell carcinoma in the rtog 0522 clinical trial. *International Journal of Radiation Oncology* Biology* Physics*, 105(2):440–447, 2019.
- Vinod Nair and Geoffrey E Hinton. Rectified linear units improve restricted boltzmann machines. In *Icml*, 2010.
- Dan Nguyen, Xun Jia, David Sher, Mu-Han Lin, Zohaib Iqbal, Hui Liu, and Steve Jiang. 3d radiotherapy dose prediction on head and neck cancer patients with a hierarchically densely connected u-net deep learning architecture. *Physics in medicine & Biology*, 64(6):065020, 2019.
- Matthew J Nyflot, Phawis Thammasorn, Landon S Wootton, Eric C Ford, and W Art Chaovalitwongse. Deep learning for patient-specific quality assurance: Identifying errors in radiotherapy delivery by radiomic analysis of gamma images with convolutional neural networks. *Medical physics*, 46(2):456–464, 2019.
- Şaban Öztürk. Convolutional neural network based dictionary learning to create hash codes for content-based image retrieval. *Procedia Computer Science*, 183: 624–629, 2021.
- Chenyang Shen, Yesenia Gonzalez, Peter Klages, Nan Qin, Hyunuk Jung, Liyuan Chen, Dan Nguyen, Steve B Jiang, and Xun Jia. Intelligent inverse treatment planning via deep reinforcement learning, a proof-of-principle study in high dose-rate brachytherapy for cervical cancer. *Physics in Medicine & Biology*, 64(11): 115013, 2019.

- Chenyang Shen, Dan Nguyen, Liyuan Chen, Yesenia Gonzalez, Rafe McBeth, Nan Qin, Steve B Jiang, and Xun Jia. Operating a treatment planning system using a deep-reinforcement learning-based virtual treatment planner for prostate cancer intensity-modulated radiation therapy treatment planning. *Medical physics*, 2020a.
- Chenyang Shen, Dan Nguyen, Zhiguo Zhou, Steve B Jiang, Bin Dong, and Xun Jia. An introduction to deep learning in medical physics: advantages, potential, and challenges. *Physics in Medicine & Biology*, 65(5):05TR01, 2020b.
- Chenyang Shen, Min-Yu Tsai, Liyuan Chen, Shulong Li, Dan Nguyen, Jing Wang, Steve B Jiang, and Xun Jia. On the robustness of deep learning based lung nodule classification for ct images with respect to image noise. *Physics in Medicine & Biology*, 2020c.
- JH Siewerdsen, IA Cunningham, and DA Jaffray. A framework for noise-power spectrum analysis of multidimensional images. *Medical physics*, 29(11):2655–2671, 2002.
- Nitish Srivastava, Geoffrey Hinton, Alex Krizhevsky, Ilya Sutskever, and Ruslan Salakhutdinov. Dropout: a simple way to prevent neural networks from overfitting. *The journal of machine learning research*, 15(1):1929–1958, 2014.
- Hossam H Sultan, Nancy M Salem, and Walid Al-Atabany. Multi-classification of brain tumor images using deep neural network. *IEEE Access*, 7:69215–69225, 2019.
- Seiji Tomori, Noriyuki Kadoya, Yoshiki Takayama, Tomohiro Kajikawa, Katsumi Shima, Kakutarou Narazaki, and Keiichi Jingu. A deep learning-based prediction model for gamma evaluation in patient-specific quality assurance. *Medical physics*, 45(9):4055–4065, 2018.
- Martin J Willemink, Holger R Roth, and Veit Sandfort. Toward foundational deep learning models for medical imaging in the new era of transformer networks. *Radiology: Artificial Intelligence*, 4(6):e210284, 2022.
- Weiwen Wu, Dianlin Hu, Wenxiang Cong, Hongming Shan, Shaoyu Wang, Chuang Niu, Pingkun Yan, Hengyong Yu, Varut Vardhanabhuti, and Ge Wang. Stabilizing deep tomographic reconstruction networks. *arXiv preprint arXiv:2008.01846*, 2020.
- Weiwen Wu, Dianlin Hu, Chuang Niu, Hengyong Yu, Varut Vardhanabhuti, and Ge Wang. Drone: Dual-domain residual-based optimization network for sparse-view ct reconstruction. *IEEE Transactions on Medical Imaging*, 2021.
- Xiaoyong Yuan, Pan He, Qile Zhu, and Xiaolin Li. Adversarial examples: Attacks and defenses for deep learning. *IEEE transactions on neural networks and learning systems*, 30(9):2805–2824, 2019.